Electronic Supplementary Information

Novel magnetic core-shell Ce-Ti@Fe_3O_4 nanoparticles as adsorbent for water contaminants removal

Ahmad A. Markeb, Laura A. Ordosgoitia, Amanda Alonso*, Antoni Sánchez, Xavier Font

ESI.1. Materials and Methods

ESI.1.1. Materials

Iron (II) chloride ($FeCl_2$), iron (III) chloride hexahydrate ($FeCl_3 \cdot 6H_2O$), sodium fluoride (NaF), titanium chloride ($TiCl_4$), cerium nitrate hexahydrate ($Ce(NO_3)_3 \cdot 6H_2O$), ammonia (NH_3) solution, and cetyltrimethyl ammonium bromide (CTAB), sodium phosphate monobasic; NaH_2PO_4, cadmium chloride ($CdCl_2$), dithizone, chloroform ($CHCl_3$), potassium cyanide (KCN), hydroxylamine hydrochloride ($NH_2Cl \cdot H_2O$) were purchased from Sigma-Aldrich, Spain. Sodium hydroxide pellets (NaOH) was purchased from Merk. Hydrochloric acid (HCl), nitric acid (HNO_3) was purchased from Panreac, SA. All the chemicals were of analytical grade or higher, and all solutions were prepared with Milli-Q water and filtered using 0.45 μm Nylon membrane filter.

ESI.1.2. Preparation magnetic Fe_3O_4 nanoparticles

Previously of Ce-Ti@Fe_3O_4 NPs (section 2.2.2), magnetite nanoparticles (Fe_3O_4-NPs) were prepared by the co-precipitation method reported elsewhere. [1] First, $FeCl_2$ and $FeCl_3 \cdot 6H_2O$, with Fe^{2+}/Fe^{3+} molar ratio of 1:2, were dissolved in 100 mL of deoxygenated ultrapure water (Milli-Q) containing 0.1% of CTAB as dispersant.

Then, the suspension was incubated for 1 hour at 40 °C and under N_2 atmosphere. Secondly, 0.6 M NH_3 solution was titrated into the iron salts solution under agitation until the pH 9.0 achieved. During titration process, the mixture's color turned from light yellow to red brown and then eventually to black which confirmed the formation of Fe_3O_4-NPs. Then, the suspension containing Fe_3O_4-NPs incubated for 1 hour under N_2 and at 40 °C. Afterwards, the NPs were washed three times using ultrapure water and magnetic decantation.

ESI.2. Characterization of the Ce-Ti@Fe_3O_4 NPs

ESI.2.1. Inductively Coupled Plasma Optical Emission Spectrometry (ICP-OES)

ICP-OES was used for the metal concentration analysis in the synthesized nanoadsorbent. Fe, Ce and Ti metals from the nanoparticles were analyzed by using ICP-OES, Perkin Elmer model Optima 4300DV. The pre-treatment of the samples consists of an acid digestion of the nanoadsorbent, dilution with MilliQ-water and filtration using 0.45 μm Nylon filters. The metal amounts are reported in terms of mg_M/g (mg of metal per mass of the nanoadsorbent) and $mmol_M/g$ (mmol of metal per mass of the nanoadsorbent). All measures were performed in triplicate. The Relative Standard Deviation (RSD) for all the measurements is 2%. Analyses were performed at Servei d'Anàlisi Química, Universitat Autònoma de Barcelona (UAB), Spain.

ESI.2.2. High Resolution Transmission Electron Microscopy (HRTEM) coupled with Energy-Dispersive Spectroscopy (EDS), and Electron Diffraction (ED) Pattern.

JEM-2011/JEOL microscope from Servei de Microscopia at UAB used to characterize the morphology and sizes of the NPs. The samples were dispersed with

ethanol and deposited on a Cu grid [2]. EDS provided the metal chemical composition of the samples based on the X-Rays emitted by an atom that has been interacted with an electron beam. Measurements were acquired with an Oxford INCA X-MAX detector [3]. Electron diffraction pattern allows studying the crystal structure of the NPs. The periodic structure of a crystalline solid acts as a diffraction grating, scattering the electrons in a predictable manner. Working back from the observed diffraction pattern, it may be possible to deduce the structure of the crystal producing the diffraction pattern [4]. Electron diffraction is also a useful technique to study the short range order of amorphous solids.

Table S1. Comparison of experimental and standard Interplanar Spacing (d) values with their respective Diffracting Plan Index (h k l) in Fe_3O_4 and Ce-Ti oxide Nanoparticles using ED pattern.

d, °A experimental	Fe_3O_4 NPs		Ce-Ti oxide NPs	
	d, °A standard	hkl	d, °A standard	hkl
3.01	2.97	220	---	---
2.74	---	---	2.73	110
2.47	2.53	311	---	---
2.20	---	---	2.23	112
2.06	2.10	400	---	---
2.04	---	---	1.94	004
1.86	---	---	1.87	201
1.77	---	---	1.73	210
1.68	---	---	1.69	211
1.56	---	---	1.58	212
1.42	1.48	440	---	---

ESI.2.3. X-Ray Diffraction (XRD)

XRD technique was used to obtain the crystalline structure of the Ce-Ti@Fe_3O_4 NPs. In a diffraction pattern, the location of the peaks on the bragg angles (2θ scale) can be compared to reference peaks. The identification of magnetite and cerium titanate were based on the characteristic peaks in the diffractograms and comparing with the database

(*Table S2*) [4-5]. Diffraction patterns were collected on Panalytical X´Pert PRO MPD (Multipurpose Diffractometer). Analyses were performed at Institut Català de Nanociència i Nanotecnologia (ICN2), Spain.

Table S.2. XRD Database reference patterns

Reference code:	00-033-0342	**Reference code:**	00-001-1111
PDF index name:	Cerium Titanium Oxide	**Mineral name:**	Magnetite
Empirical formula:	Ce0.66O2.98Ti	**Empirical formula:**	Fe3O4
Chemical formula:	Ce0.66TiO2.975	**Chemical formula:**	Fe3O4
		PDF index name:	Iron Oxide

Table S.3 Comparison of experimental and standard (2θ) values with their respective Diffracting Plan Index (h k l) in Fe_3O_4 and Ce-Ti oxide NPs using XRD pattern

2θ experimental	**Fe_3O_4 NPs**		**Ce-Ti oxide NPs**	
	2θ standard	**hkl Diffraction plan**	**2θ standard**	**hkl Diffraction plan**
23.13	---	---	25.82	101
31.42	30.06	220	---	---
32.85	---	---	32.74	110
35.77	35.45	311	---	---
40.44	---	---	40.45	112
43.64	43.04	400	---	---
47.14	---	---	46.82	004
52.98	---	---	52.98	210
57.45	57.17	511	---	---
58.42	---	---	58.44	212
63.18	62.73	440	---	---
68.63	---	---	68.40	024
78.05	---	---	77.90	106
87.29	86.91	642	---	---
90.20	89.93	731	---	---

ESI.2.4. Scanning Transmission Electron Microscopy (STEM) coupled with Electron Energy Loss Spectra (EELS)

The morphology of the core-shell nanocomposite was estimated by STEM coupled with HAADF detector and EELS. Images were acquired using an FEI Tecnai G2 F20 microscope operated at 200 kV and equipped with a GIF Quantum energy filter. All spectra were recorded using a convergence semiangle of about 12 mrad and a collection semiangle of about 40 mrad. EDX spectra were obtained using an EDAX super ultra-thin window (SUTW) X-ray detector. The sample was first dispersed in ethanol and sonicated, then deposited onto the copper microscopy grid coated with an amorphous carbon film. By imaging with the electrons that have an energy loss corresponding to core losses of particular elements using STEM, one can obtain elemental information with high spatial resolution. A full energy loss spectrum from a series of points across the particle in a STEM configuration, which allows the extraction of linear compositional variation was used to obtain chemical information about the nanostructure. Analyses were performed at Institut Català de Nanociència i Nanotecnologia (ICN2), Spain.

ESI.2.5. UV/VIS and luminescence spectra analysis

Absorption and luminescence spectra of Ce-Ti@Fe_3O_4 NPs were performed to estimate the valency of the cerium in the NP and confirm its speciation. Absorption and luminescence spectra were analyzed using UV/Vis spectrophotometer, Cary 50 bio Varian, and Luminescence spectrometer, LS 55 Perkin Elmer. pH was adjusted using Crison pH meter 2001. Samples are prepared by suspension of 1 g of the core-

shell nanomaterial in 1 L Milli-Q water adjusted to pH 7.0 using 0.1M NaOH.

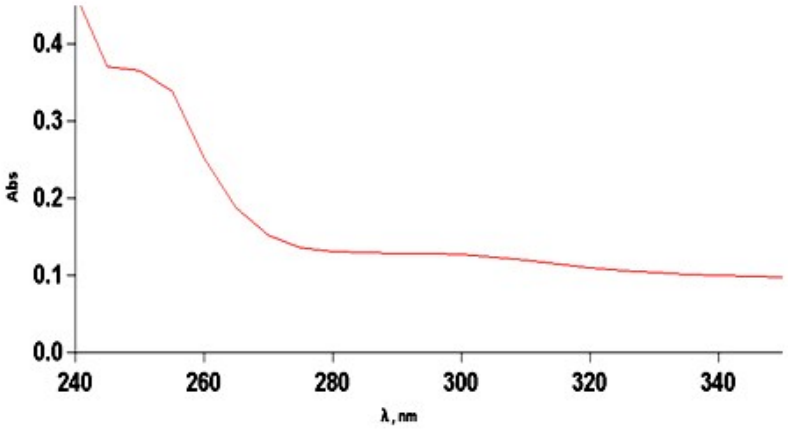

Figure S.1. UV/Vis spectra for Ce-Ti@Fe_3O_4 nanomaterial.

Although the main absorption band is around 310 nm for Ce(III), characteristic broad bands in the UV region between 330 and 200 nm could be observed due to the coexistence of Ce(III) and Ce(IV) species because of its particular electronic configuration. [6]

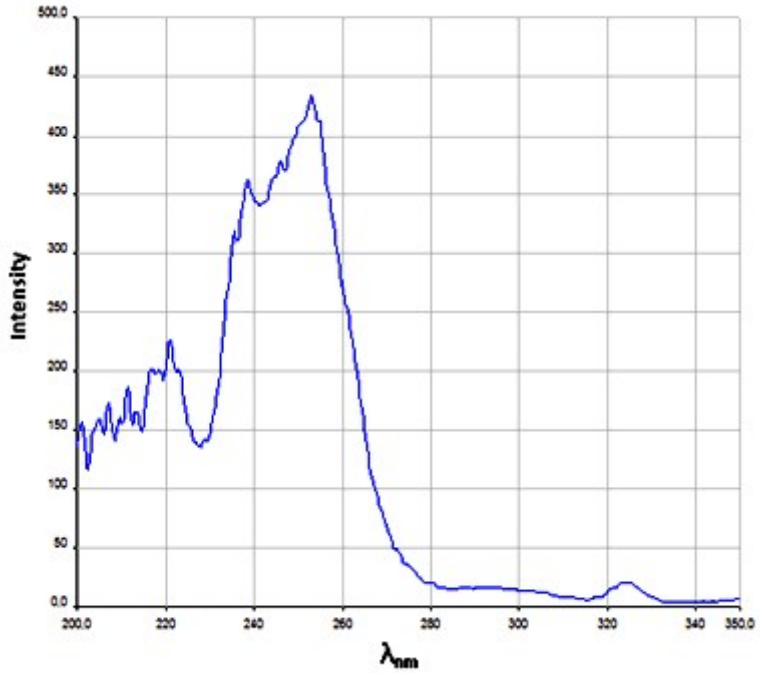

Figure S.2. Luminescence spectra of the Ce-Ti@Fe_3O_4 nanomaterial at the excitation spectrum for λ_{em}=363 nm and the emission spectrum recorded upon λ_{exc}=266 nm.

ESI.3. Analytical methods used in the Adsorption Experiments

ESI.3.1. Ionic chromatography (IC) for fluoride, nitrate and phosphate analysis

The determination of phosphate, as phosphorous (PO_4-P), Fluoride anion (F^-) and nitrate (NO_3-N) was determined using ICS-2000 (Dionex) ion chromatographic system, with ultimate 3000 autosampler. An ion exchange column specifically designed for rapid analysis of inorganic anion (Dionex IonPac AS18, 4 x 250 mm) equipped with an IonPac guard column (Dionex IonPac AG18, 4 x 50 mm) was used. Chromeleon® software was used to acquire data and control the instrumentation. Standard error in the measurements is < 0.1%.

A stock solution of each contaminant was prepared by dissolving the appropriate amount of its precursor in ultrapure water. All working contaminants solutions for calibration curve and adsorption studies were prepared by diluting the stock solution. Calibration standards and samples were filtered using 0.45 μm Nylon membrane filter before injection.

ESI.3.2. UV-Vis for Cadmium analysis

Calibration curves for cadmium were constructed using 99.995% cadmium(II) chloride by using a colorimetric method, based on the reaction of cadmium with dithizone to form a complex that is extracted with chloroform. Then the absorbance is measured at 518nm [7]. Cadmium stock solution was prepared by dissolving the appropriate amount in 5 % nitric acid. The cadmium solutions for calibration curve and adsorption studies were prepared by diluting the stock solution.

ESI.4. Adsorption experiments procedure

Batch adsorption tests were used to determine the adsorption efficiency by the synthesized NPs. A contaminant solution with an initial concentration (C_0) (mg/L) was prepared as mentioned before (section 2.4.1). A concentration of adsorbent (W) (g/L) was added into a conical flask containing 25 mL of the aqueous contaminated solution. pH of the solution was adjusted when necessary using 0.1 M NaOH and/or HCl until pH 7. The flask was shaken (200 rpm) at 25 °C using a thermostat shaker. Residual contaminant concentration in the solution after 24h of adsorption, C_e, was determined by the corresponding analytical method detailed in Section 2.4. Equilibrium adsorption capacity, Q_e, of the adsorbent was calculated as Equation S.1:

$$Q_e = (C_0 - C_e)/W \quad (1)$$

Adsorption experiments were preformed using different initial concentrations for each contaminant where based on the reported typical concentration in water or on the maximum contaminated level (MCL). For instance, phosphate initial concentration tested was 10 mg/L due to municipal wastewater may contain 4-15 mg/L, and domestic wastewater may contains 10-30 mg/L [1a]. Furthermore, 10 mg/L initial fluoride concentration was selected due the maximum contaminated level in water is 1.5 mg/L [8] but, it has been reported that the fluoride concentrations in groundwater range from well under 1.0 mg/L to more than 35.0 mg/L in several regions of India.[9] In addition, the initial nitrate concentration tested is 50 mg/L due to according WHO guidline the MCL is 50 mg/L [8b]. Also, 10 mg/L intial cadmium coencentration was selected due to wastewater contains 10 – 100 mg/L of cadmium contaminant [10]. All the experiments were performed at pH 7 as a typical value in real media.

Table S.2 Adsorption capacities and removal efficiencies values for contaminants removal from the literature

Pollutant	Nanoadsrbents	Initial concentration, mg/L	Dose, g/L	Q_e, mg/g	Removal, %	Ref.
PO_4-P	Ce-Ti@Fe_3O_4	10	0.90	**11.10**	**99.90**	This work
	C100@Fe_3O_4	10	1.0	3.60	36.00	[1a]
	$Al(OH)_3$	10	2.32	2.46	57.07	[11]
	Fe_3O_4	10	10.0	0.88	88.00	[12]
F	Ce-Ti@Fe_3O_4	10	0.97	**10.31**	**100.0**	This work
	$Al(OH)_3$	10	1.60	5.74	91.84	[13]
NO_3-N	Ce-Ti@Fe_3O_4	50	1.0	**42.50**	**85.00**	This work
	Rice straw activated carbon	50	1.0	9.00	18.00	[14]
Cd^{2+}	Ce-Ti@Fe_3O_4	10	1.0	4.53	45.28	This work
	Cork biomass powder	10	1.0	6.40	64.48	[15]

References

1(a) A. Abo Markeb, A. Alonso, A. D. Dorado, A. Sánchez and X. Font, *Environmental Technology*, 2016, 1; (b) S. Laurent, D. Forge, M. Port, A. Roch, C. Robic, L. Vander Elst and R. N. Muller, *Chemical Reviews*, 2008, **108**, 2064.

2 A. Alonso, N. Vigues, X. Munoz-Berbel, J. Macanas, M. Munoz, J. Mas and D. N. Muraviev, *Chemical Communications*, 2011, **47**, 10464.

3 A. Alonso, A. Shafir, J. Macanás, A. Vallribera, M. Muñoz and D. N. Muraviev, *Catalysis Today*, 2012, **193**, 200.

4 L. G. Berry and R. M. Thompson, *Waverly Press: New York*, 1962, 194.

5 J. L. Zhang, R. S. Srivastava and R. D. K. Misra, *Langmuir*, 2007, **23**, 6342.

6 K. Annapurna, R. N. Dwivedi, P. Kundu and S. Buddhudu, *Materials Letters*, 2004, **58**, 787.

7(a) A. R. Contreras, A. García, E. González, E. Casals, V. Puntes, A. Sánchez, X. Font and S. Recillas, *Desalination and Water Treatment*, 2012, **41**, 296; (b) G. A, C. J and J. D, *American Public Health, Association, American Water Works, Association, Water Environment Federation*, 2005, **21st edition**.

8(a) WHO, 2006, **1 third edition, Geneva**, 375; (b) p. i. Drinking-water, *WHO*, 2004.

9 Meenakshi and R. C. Maheshwari, *Journal of Hazardous Materials*, 2006, **137**, 456.

10 Y. Yurekli, *Journal of Hazardous Materials*, 2016, **309**, 53.

11 P. H. Hsu and D. A. Rennie, *Canadian Journal of Soil Science*, 1962, **42**, 197.

12 G. T. T. Le and P. Sreearunothai, *4th International Conference on Informatics, Environment, Energy and Applications (IPCBEE)*, 2015, **82**.

13 B. Shimelis, F. Zewge and B. S. Chandravanshi, *Bull. Chem. Soc. Ethiop.*, 2006, **20**, 17.

14 S. M. Yakout and A. A. Mostafa, *Journal of Animal and Veterinary Advances*, 2014, **13**, 728.

15 F. Krika, N. Azzouz and M. C. Ncibi, *Arabian Journal of Chemistry*.